COBEM 2023 27TH INTERNATIONAL CONGRESS OF MECHANICAL ENGENEERING

ABCM Brazilian Society of Mechanical Sciences and Engineering
27th ABCM International Congress of Mechanical Engineering
December 04-08, 2023, Florianópolis-SC, Brazil

COB-2023-0563
TRANSIENT BEHAVIOR OF DIFFUSION FLAMES: BUOYANCY INDUCING FLICKERING IN GROOVE GEOMETRY

[a] **Guilherme Gonçalves Alvarez**
[a] **Eduardo Reis Sampaio Filho**
[b] **Fernando Fachini Filho**
[a] **Leandro Marochio Fernandes**

[a] Instituto Federal de Educação, Ciência e Tecnologia do Espírito Santo - Campus Cachoeiro de Itapemirim, Rodovia ES-482 Fazenda Morro Grande, 29311-970 Cachoeiro de Itapemirim - ES, Brazil
guilherme.alvarez@hotmail.com, engmec.eduardorsf@gmail.com, leandro.mfernandes@ifes.edu.br

[b] Grupo de Mecânica de Fluidos Reativos, Coordenação de Pesquisa Aplicada e Desenvolvimento Technologico - COPDT, Instituto Nacional de Pesquisas Espaciais INPE, 12630-000 Cachoeira Paulista/SP, Brazil
fachiniff@gmail.com

Abstract. *This work describes the flickering phenomenon in groove diffusion flames, using a bi-dimensional flame model to analyze the influence of a large aspect ratio on the oscillation frequency. Diffusion flames present a particular transient behavior characterized by an oscillation along the flow direction with a specific range of frequencies. The flickering phenomenon occurs due to a global instability generated by the annular buoyancy flow induced by combustion heat release. The instability analyses done so far consider axisymmetric flames, e.g. jet flames and cylindrical pool fires. To study flames that present a parallel flow, the groove flame configuration was chosen. It consists of a rectangular pool fire with a large aspect ratio, a geometry that permits the occurrence of a bi-dimensional flow. The physical model considers the fuel stream depending only on the heat transport to the liquid surface. It also considers the Burke-Schumann limit. To validate the theoretical solution, the flickering frequencies are measured in grooves of different aspect ratios. The experimental setup consists of a coif, a test cell, and a suspended base, with a honeycomb in the entry of the setup in order to laminarize the incoming flow induced by the buoyant force. Image analysis is the technique applied to measure flame oscillation. This method is based on video recording of the flame captured by a digital camera, which is divided into frames to perform the analysis. N-heptane is used in the experiment due to its flame generating favorable images to the process and the data availability. The flame height in each frame is measured, which permits following its evolution and consequently determining the oscillation frequency. The measurements show the burning regime (flickering and puffing) and that the flame oscillation frequency depend on the groove width. For the groove with an aspect ratio of* $2/5$ *the flame exhibits the flickering phenomenon and its frequency is* $11.81Hz$*. However, between the aspect ratios* $2/5$ *and* $3/5$*, and the flickering disappears and puffing is observed, the frequency drops to* $7.6Hz$*. For the lowest aspect ratio* $(4/5)$*, which is almost a square container, the frequency decreases slightly* $(6.8Hz)$*. Furthermore, due to hydrodynamic instability, the flame surface is disturbed with a spatial average flame height of 67 mm. A simplified model (infinitely fast chemical kinetics, constant transport and thermodynamic coefficients, and unitary Lewis number) is developed which is able to represent qualitatively a flame height of 91mm.*

Keywords: *flickering, puffing, groove flame, diffusion flame, aspect ratio*

1. INTRODUCTION

Diffusion flames present an intrinsic transient behavior characterized by an oscillation along the flow direction with a specific range of frequencies. The flickering phenomenon occurs due to an instability generated by the annular buoyancy flow induced by heat (Chamberlin and Rose, 1948). Such unstable flow is not much sensitive to factors like the size of the burner nozzle, the type of gas fuel, or the flow rate, as shown in research made for jet flames (Buckmaster and Peters, 1986) . The instability is also independent of the volumetric heat released rate (Cetegen and Kasper, 1996). Those characteristics of independence are related to the fact that the diffusion flame flickering presents a frequency that does not vary too much. For jet diffusion flames with burner nozzle diameter in the order of 10^{-2} to 10^{-1} meters, the frequency varies in a range of 10 Hz to 20 Hz (Chen *et al.*, 1988; Buckmaster and Peters, 1986). Those data show the peculiarity of the phenomenon and the difficulty of finding a good description of the instability that generates it, reasons for the great variety of hypotheses presented in the literature for years to explain the facts (Jiang and Luo, 2000).

The flickering phenomenon was first described in detail by Chamberlin and Rose (1948). The authors took several sequenced pictures of flames burning and made a qualitative-quantitative analysis, a methodology called the photographic

method. It was observed that for any flame without a primary air supply and burning in any kind of nozzle, the basis of the flame remains stable, while its medium portion moves in and out and its top moves up and down, both in a periodical pattern. Paying attention only to the top portion, it's notable that the upward movement takes a longer time than the downward movement.

This observation is in agreement with the flickering mechanism as it's currently understood. The oscillation actually occurs due to the local extinction of the flame caused by the flame stretching imposed by the vortices (Moreno-Boza *et al.*, 2016). Hence, the frequency of flickering is in the same order of magnitude as the convective time associated with those vortices (Cetegen and Kasper, 1996), indicating that the frequency data is an adequate parameter for the understanding of the instability.

Several analyses were made to understand the nature of those vortices. For jet diffusion flames in burners of small diameter, it was observed a velocity profile characterized by a Poiselle flow near the tube, the velocity modulus decreases with the distance but turning to increase, presenting a local maximum in some radius; This velocity profile indicates the existence of the surrounding buoyant flow in the flame (Buckmaster and Peters, 1986), while the Poiselle distribution is associated with the jet flow. This way, two types of flows coexist in this kind of flame, each one presenting a different type of instability. In the jet flow, a cylindrical train of relatively small vortices is associated with a Kelvin-Helmholtz instability, born in the shear layer between the fuel jet and the atmosphere (Liñan *et al.*, 2015). This train is not observed for flows with Froude number smaller than unity, due to the prevalence of buoyancy in the global flow (Jiang and Luo, 2000). By contrast, a train of large vortices is observed in the buoyant flow, which are bigger than those inner vortices (Chen *et al.*, 1988).

The analysis of Buckmaster and Peters (1986) suggested that those large vortices came from a modified type of Kelvin-Helmoholtz instability, since the several inflection points presented in the velocity profile. The authors made an inviscid stability analysis assuming the approximation of a nearly parallel flow to the annular flow surrounding the flame. But, both of the approximations carry on several errors in the analysis (Moreno-Boza *et al.*, 2016). A posterior numerical work made by Jiang and Luo (2000), shows that the instability was independent of small perturbations on its onset, proving that it can not be a shear layer instability.

Another hypothesis for the instability formation is the density stratification found around the flame, the instability is of a Rayleigh-Taylor type (Cetegen and Kasper, 1996). For axisymmetric plumes, the flow near the flame axis is buoyant-accelerated downstream, originating a toroidal vortex that progresses and perturbs the upstream flow, following a vortex-induction feedback mechanism. Those perturbations grow fast due to the action of gravity, allowing the vortex to reach a bigger diameter without a long train, which will not occur in the case of Kelvin-Helmholtz instability. In fact, the vortex train begins at a height of one-half of the diameter of the nozzle. The model of Cetegen and Kasper seems to scale very well with the experimental results done in several different types of buoyant flames, especially pool fires.

Finally, most recent analyses of the phenomena shows that the instability of the buoyant flow is a self-sustaining instability. A linear stability analysis done by Liegens *et al.* (1996), validated with experiments, shows that a local absolute instability, whose onset is at the burner rim, is responsible for the observed coherent flow. The oscillations generated goes upstream and downstream, influencing all the surrounding of the flame (Liegens *et al.*, 1996). The inflection points observed in the velocity profile, rather than responsible for a shear layer instability, are actually correlated to the characteristics of a globally unstable flow. The authors identify that the absolute instability emerges after a transitional point, in which a convective instability gives place to it. The work of Maxworthy (1999) sustains this hypothesis. It shows that, in the burner rim, the velocity is zero while the temperature is high, something that may only occur in an absolute instability. Downstream, the velocity is too high to be associated with a convective instability, also proving the absolutely unstable flow hypothesis.

Despite the phenomena described until now remains associated with jet flames, the same characteristics are physically similar to pool fires flickering (Moreno-Boza *et al.*, 2018). A specific kind of pool fire configuration is the groove flame. It consists of a rectangular pool fire with a large length in comparison to its width, a geometry that permits the occurrence of a rectangular bi-dimensional flow. The toroidal vortices of the annular flow, presenting a circular section in jet flames, now assume an elliptical section with semi-major axis much larger than the semi-minor axis. Also, for larger aspect ratios, it's possible to consider that the lateral vortices are two parallel cylinders, each one on each side of the flame. Those physical characteristics distinguish the groove flame as a flame that is simple to study analytically. Furthermore, the description of this kind of flame is relevant given its application for fuel storage.

2. SCALE ANALYSIS

Given the flame specifications, an estimate for the vertical velocity v_c in the natural convection can be found, imposing the Froude number equal to one. The estimate is determined considering the flame length l_f as a multiple (n) of the groove width l_g, i.e. $l_f = nl_g$, and the gravitational acceleration g:

$$Fr = \frac{v_c}{\sqrt{gl_f}} = \frac{v_c}{\sqrt{gnl_g}} \sim 1 \implies v_c \sim \sqrt{gnl_g} \tag{1}$$

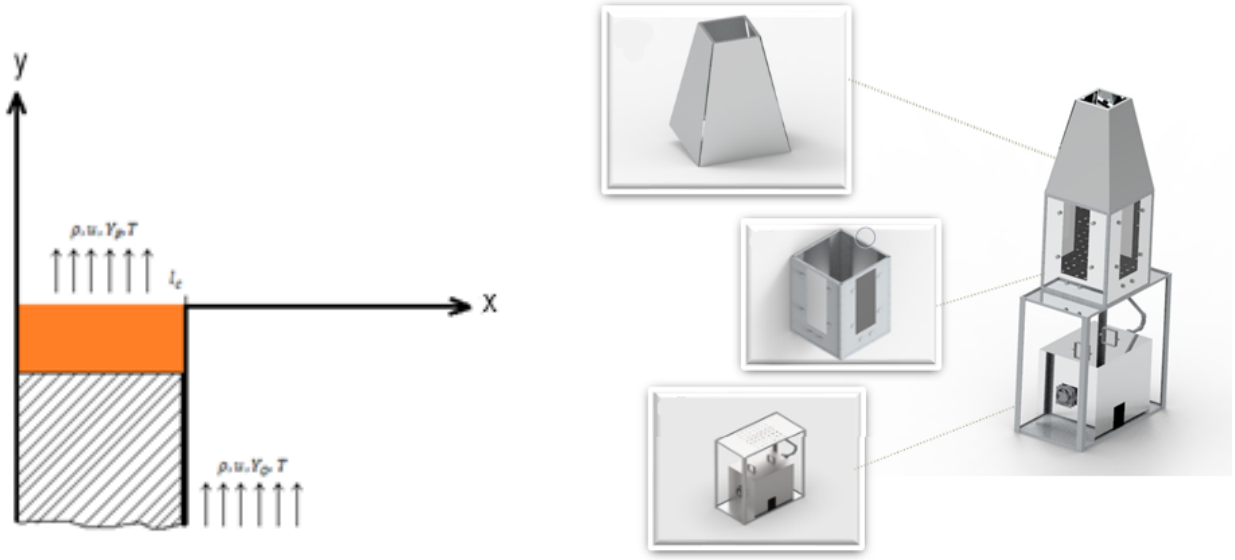

(a) (b)

Figure 1. a) Schematic drawing of the channel with liquid fuel, i.e. groove burner. The coordinate system is at the center of the channel and on the liquid surface which is kept unchanged; b) Experiment structure diagram.

Between the hot gases inside the flame and the cold resting atmosphere, there is a shear layer, whose width is

$$\delta \sim \frac{l_f}{\sqrt{Re}} \implies \frac{\delta}{l_g} = \frac{n}{\sqrt{Re}} \tag{2}$$

in which the Reynolds number is based on the groove width $Re = l_g v_c/\nu$.

From the mass conservation equation, the estimated vertical component of the velocity v_c, Eq. (1), and the estimated shayer layer thichness, Eq. (2), the horizontal component of the velocity u_c can be estimated. The variation of the vertical component of the velocity, v_c, in a distance of l_f, and the variation of the horizontal component of the velocity, u_c, in the distance equal to the shear layer width δ, are related by

$$\frac{u_c}{\delta} \sim \frac{v_c}{l_f} \implies u_c \sim \frac{\delta}{l_f} v_c = \frac{v_c}{\sqrt{Re}} = \frac{\nu^{1/2} g^{1/4} n^{1/4}}{l_g^{1/4}} \tag{3}$$

The horizontal component of the convection brings the oxidizer from the ambient to close to the flame, which increases the oxidant gradient around the flame, increasing, then, the oxidant flux to it. Besides, the horizontal component of the velocity u pushes the vortex created at the flame base to its center, meanwhile it displaces to the flame tip.

So, when the vortex influence arrives at the flame center, the stretch can extinguish or not the flame, depending on the flame height this occurs.

In the case of not occurring the extinction, the flame length only oscillates. It is the flickering phenomenon. But, if it occurs, the flame is separated in two. It is the puffing phenomenon (Moreno-Boza *et al.*, 2018). The flame portion attached to the groove is controlled by the fuel vaporization, but the fuel pocket separated from the main flame continues burning meanwhile it is taken by the flow.

3. MATHEMATICAL FORMULATION

This study considers an "infinite" groove, which justifies an bidimensional model. The groove length is $2l_c$, filled with ethanol (C_2H_5OH), in an atmospheric environment with oxidizer mass fraction $Y_{O\infty}$, density of ρ_∞, and temperature of T_∞. By adopting bilateral symmetry with respect to the vertical axis (y-axis) and positioning the horizontal axis (x-axis) aligned with the fluid surface, the proposed configuration is obtained (Figure 1a). The flow field imposed by the liquid-gas phase change is one dimensional

The physical model is rescalled with the characteristic variables, then,

$$St\partial_t \rho + \nabla \cdot (\rho \vec{v}) = 0 \quad , \tag{4}$$

$$St\partial_t (\rho \vec{v}) + \nabla \cdot (\rho \vec{v}\vec{v}) = -\frac{1}{\gamma (Ma)^2} \nabla p + \frac{1}{Re} \nabla \cdot \vec{\vec{\tau}} + \frac{1}{(Fr)^2}(1-\rho) \quad , \tag{5}$$

$$St\partial_t(\rho Y_i) + \nabla \cdot (\rho \vec{v} Y_i) = \frac{1}{PeLe_i}\nabla \cdot (\rho \mathcal{D}_i \nabla Y_i) + s_i Da\omega \quad , \tag{6}$$

$$St\partial_t(\rho h) + \nabla \cdot (\rho \vec{v} h) = \frac{\gamma - 1}{\gamma}\left(St\partial_t p + \vec{v} \cdot \nabla p\right) + \frac{Ma^2(\gamma - 1)}{Re}\nabla \vec{v} : \vec{\vec{\tau}} + \frac{1}{Pe}\nabla \cdot (k\nabla T) - QDa\omega \tag{7}$$

The principles of conservation (mass, momentum, species, and energy in the form of enthalpy) are represented by Eqs. (4) to (7) respectively, where $\vec{v}$ is velocity, p is pressure, Y_i is the mass fraction of species i, h is sensible enthalpy, and the molecular transport coefficients are represented by D_i for mass diffusivity of species i and k for thermal diffusivity.

In the set of obtained equations, certain dimensionless numbers are presented. These include the Strouhal number, $St \coloneqq (\hat{l}_c/\hat{v}_c)/\hat{t}_c$,which relates the residence time to the characteristic time of the addressed problem. The Mach number, ($Ma \coloneqq \hat{v}_c/\hat{a}$), measures the flow velocity relative to the speed of information propagation in the flow. Lastly, the Reynolds number, ($Re \coloneqq \hat{l}_c\hat{v}_c/\hat{\nu}_c$), quantifies the flow characteristics in relation to viscosity and inertia, where ν represents cinematic viscosity. The Froude number, ($Fr \coloneqq \hat{v}_c/(\hat{g}\hat{l}_c)^{1/2}$), relates the inertial and body forces of the system, with g being the acceleration due to gravity. The Péclet number, ($Pe \coloneqq \hat{l}_c\hat{v}_c/\hat{\alpha}_c$), a relation between the heat conduction time and the residence time of the system, where $\hat{\alpha}$ represents thermal diffusivity. The Lewis number ($Le_i \coloneqq \hat{\alpha}_c/\hat{\mathcal{D}}_{ic}$) represents the ratio of mass diffusion to heat diffusion. Lastly, the Damköhler number ($Da \coloneqq \hat{l}_c B Y_{Oc}/\hat{V}_c$) provides the relationship between residence time and chemical reaction time (where B is the pre-exponential factor of the reaction).

Eqs. (6) for $i = F,\ O$, and these two species conservation equations and (7) according to Shvab (1948) and Zeldovich (1951).

Note that $\mathcal{C} \coloneqq (S + 1)/Q$, and $S \coloneqq \hat{s}\hat{Y}_{Fc}/\hat{Y}_{O\infty}$ - with s being the stoichiometric coefficient of the single-step and irreversible chemical reaction represented by $F + \hat{s}O_2 \rightarrow (1 + \hat{s})P$ - and $Q \coloneqq \hat{q}\hat{Y}_{F,c}/(\hat{c}_{p,c}\hat{T}_c)$ - with $\hat{q}$ representing the heat of combustion and $\hat{c}_p$ the specific heat at constant pressure. In the chemical reaction, F denotes the fuel; O_2, the oxygen; and P, the products.

The boundary conditions for the fuel medium are imposed as follows:

On the symmetry axis ($x = 0, \forall y$):

$$\partial_x T = \partial_x u = \partial_x v = \partial_x Y_F = \partial_x Y_O = 0 \tag{8}$$

On the liquid surface ($x \leq 1, y = 0$):

$$T = T_b,\ v = v_b,\ u = 0,\ Y_F = Y_{Fb},\ \partial_y T = \rho_b v_b L,\ \ \partial_y Y_F = \rho_b u_b (1 - Y_{Fb}) \tag{9}$$

Outside the liquid surface ($x \geq 1, y = 0$):

$$T - 1 = \rho - 1 = u - 1 = Y_F = Y_O - 1 = 0 \tag{10}$$

At the boundaries of the experimental environment:

$$\partial_x T = \partial_x u = \partial_x v = \partial_x Y_F = \partial_x Y_O = 0 \quad \text{for } x = D, -D \leq y \leq D \tag{11}$$

$$\partial_y T = \partial_y u = \partial_y v = \partial_y Y_F = \partial_y Y_O = 0 \quad \text{for } 1 < x \leq D,\ y = -D, D \tag{12}$$

The values of the length and width of the experiment cell D is given in the next section.

Equations for the transport of two additional scalars were derived by combining Eqs. (6) for $i = F,\ O$, and these two species conservation equations and (7) (Shvab, 1948; Zeldovich, 1951). These equations were developed for equidiffusive reactants, density constant, uniform flow field, estacionary, and constant transport coefficient, i.e. Burke-Schumann model (Burke and Schumann, 1928). In this way, the mixture fraction variable $Z \coloneqq SY_F - Y_O + 1$ and the enthalpy excess $H \coloneqq \mathcal{C}T + Y_F + Y_O$ are used because the chemical reaction nonlinear term ω is eliminated (Liñán and Williams, 1993; Liñán, 2001; Fachini, 1999; Fachini *et al.*, 1999; Fachini, 2007), and the resulting equations for this problem are

$$\frac{\partial \Psi_i}{\partial y} = \frac{1}{Pe}\frac{\partial^2 \Psi_i}{\partial x^2} \tag{13}$$

with $\Psi_1 = Z$ and $\Psi_2 = H$.

Once Eqs. (13) and (14) are solved, it is sufficient to determine the contour curve $Z = 1$, i.e., where the mixture fraction (Z) takes on the unit value, in order to find the location of the flame front. Furthermore, the temperature distribution is given by:

$$T = \frac{1}{\mathcal{C}}\left[H - \frac{Z-1}{S}\right] \ \text{(for } Z > 1), \qquad T = \frac{1}{\mathcal{C}}\left[H + (Z-1)\right] \ \text{(for } Z < 1) \tag{14}$$

Regarding the boundary conditions of the problem, it is known that on the surface of the liquid fuel, it is heated to the boiling temperature T_b and vaporized at a rate proportional to the heat flux from the flame (The subscript "b" denotes the conditions of the vaporized fuel). To simulate the fuel flux provided by the liquid vaporization, it is assumed the oxidizer flow with the same velocity of the fuel flow. Besides, the analytical solution of Eqs. (13), the reactants flow must be inside a channel, which has the width $x = d$ and at that position $Z = H - H_\infty = 0$. Then, the solution of Eqs. (13) is (Lin *et al.*, 1986)

$$Z = \sum_{n=0}^{N} 4(S+1)\frac{sin(\Lambda_n)}{2\Lambda_n + sin(2\Lambda_n)} cos(\Lambda_n x) exp\left(-\frac{\Lambda_n^2 y}{Pe}\right) \tag{15}$$

with $\Lambda_n = [(1/2+n)(\pi/d)]$ and satisfying condition of symmetry in the y-axis and $\Psi_1 = Z(0 \leq x \leq 1, y = 0) = 1$ ($Y_F = Y_O = 0$) at the liquid surface. Therefore, the flame length at the center of the groove is

$$\frac{1}{4(S+1)} - \sum_{n=0}^{N} \frac{sin(\Lambda_n)}{2\Lambda_n + sin(2\Lambda_n)} exp\left(-\frac{\Lambda_n^2 y_f}{Pe}\right) = 0 \tag{16}$$

For ethanol ($S = 5$) and the conditions such that $Pe = 4.5$, the flame height y_f is 12.18 ($\hat{y}_f = 91.35mm$). The mean of the flame height for the aspect ratio $1/5$ is $67mm$. Considering the forced convection, condition considered in the mathematical model, leads to higher flame heights, the model is capturing the main processes.

4. EXPERIMENTAL SETUP

This work consists of a modification of the "pool fire" experiment (Liu *et al.*, 2020), i.e., the liquid fuel is kept at constant level (ullage zero) and in a rectangular geometry. Two fuels (alcohol and n-heptane) were used in the experiments. Since alcohol burns cleaner than the n-heptane, the visualization of the alcohol diffusion flame is difficult. The alcohol tests are used as qualitative data, meanwhile the n-heptane flames were employed to analyse the transient phenomenon (flicketing and/or puffing).

The fuel-filled groove is positioned inside a partially enclosed structure (test cell) to eliminate undesirable external influences (e.g., perturbed air flow). The experimental setup can be divided into 3 main parts (i) the structure has a coif with dimensions $490\ mm \times 490\ mm$ and $150\ mm \times 150\ mm$ for the lower and upper sections, respectively, and a length of $650\ mm$, as seen in Fig. (1b); (ii) the test cell with a square section of $490\ mm \times 490\ mm \times 650\ mm$, in which the groove is placed; and (iii) the table with dimensions $900\ mm \times 500\ mm \times 950\ mm$. The flow laminarization device consists of two layers of metal mesh screens, covering the entire section of the test cell, spaced at $75\ mm$ apart, and a 50 mm layer of steel wool between them, positioned between the table and the test cell.

The grooves differ in their aspect ratio, i.e., the ratio between width and length. Two groups of grooves were tested, the first one considered lengths were 2, 5, 10, and 20 times the width ($15\ mm$). The second group it was fixed the length ($75\ mm$), varying the width in the aspect ratios $2/5$, $3/5$, $4/5$ and 1.

The measurement technique consists of image analysis based on video recording of the flame captured by a digital camera, which is divided into frames. Thus, the flame height in each individual picture is measured and compared.

5. RESULTS

Some images were selected from the video, showing the time instant of lowest and highest flame heights during the flickering cycle. The difference between the two heights are significant for every aspect ratio. Thus, the flickering frequency was easily captured as seen in Figs. (2) to (5). These figures put in evidence also the spatial variation of the flame height. The wave number is linearly dependent of the aspect ratio: for the aspect ratio 1/2, the wave number is half; for $1/5$ the wave number is 3/2; for $1/10$ the wave number is 5/2; for 1/20 the wave number is 7/2.

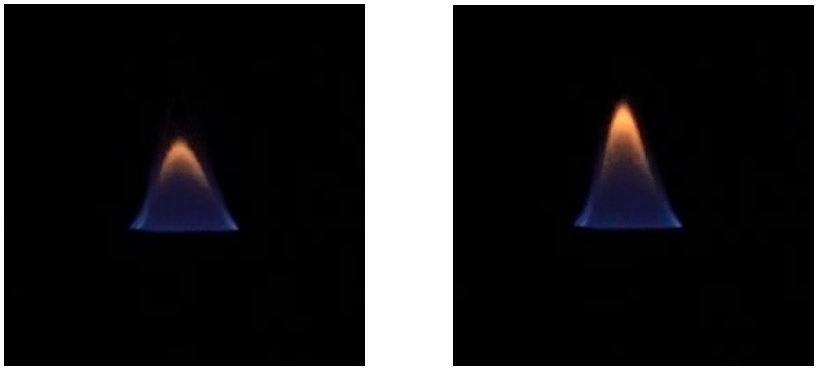

(a) Shorter height (b) Greater height

Figure 2. Groove of aspect ratio $1/2$

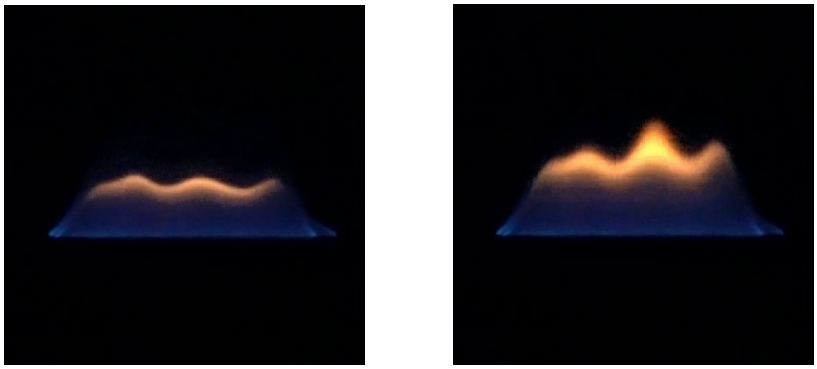

(a) Shorter height (b) Greater height

Figure 3. Groove of aspect ratio $1/5$

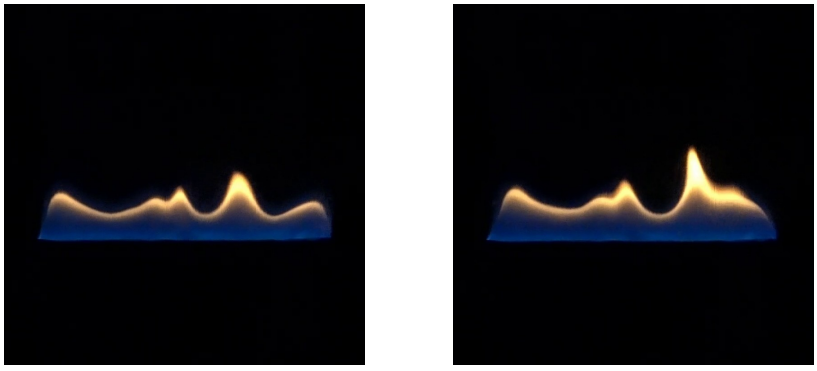

(a) Shorter height (b) Greater height

Figure 4. Groove of aspect ratio $1/10$

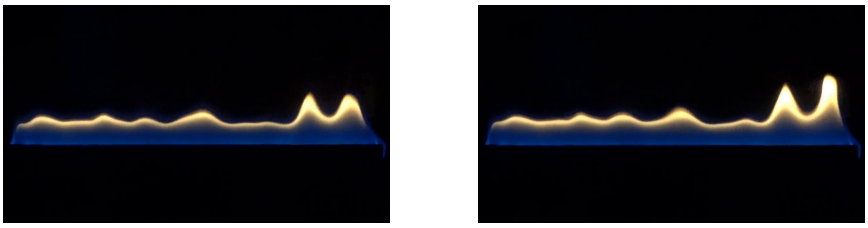

(a) Shorter height (b) Greater height

Figure 5. Groove of aspect ratio $1/20$

The results are presented only for the follwing aspect ratios: 1/2, 1/5 and 1/10, and for each one, three tests were

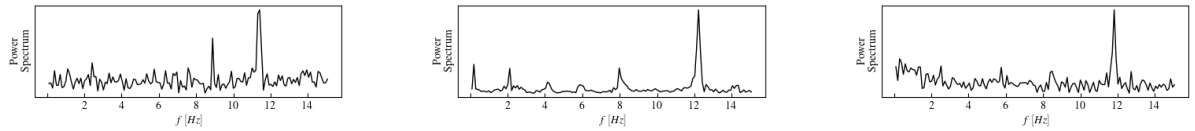

(a) (b) (c)

Figure 6. Frequency measurement for aspect ratio $1/2$ (15 mm x 30 mm groove): frequency of a) 11.41 Hz, b) 12.22, and c) 11,81 Hz. The mean frequency is $11.81\ Hz$.

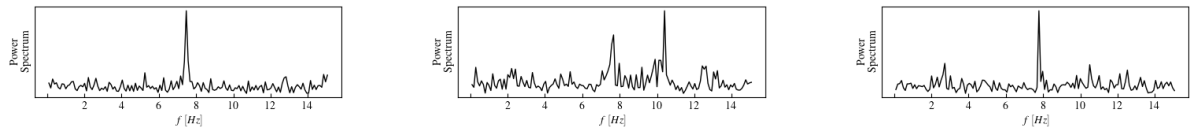

(a) (b) (c)

Figure 7. Frequency measurement for aspect ratio $1/5$ (15 mm x 75 mm groove): frequency of a) 7.47 Hz, b) 7.67, and c) 7.77 Hz. The mean frequency is $7.63\ Hz$.

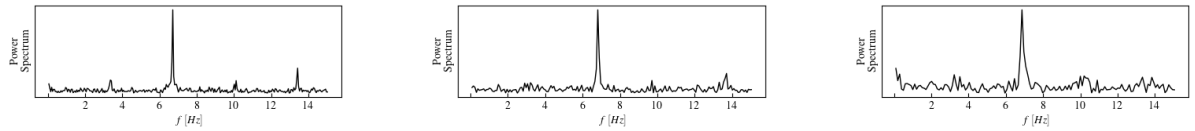

(a) (b) (c)

Figure 8. Frequency measurement for aspect ratio $1/10$ (15 mm x 150 mm groove): frequency of a) 6.71 Hz, b) 6.81, and c) 6.86 Hz. The mean frequency is $6.79\ Hz$.

conducted. A main frequency and harmonics were identified at the $1/2$ and $1/5$ aspect ratios. As the aspect ratio decreases the harmonics tend to disappear.

For the 1/5 aspect ratio, only flickering was identified, and, for the other two grooves, puffing is observed. The change of the aspect ratio from $1/5$ to $1/10$ is the transition from flickering to puffing, and clearly the frequencies of these two phenomena are close to the factor 2. Once the puffing starts controlling the periodic behavior of the flame, the frequency becomes less sensitive to the aspect ratio.

Note that there is a higher frequency in Fig.(7b) than those observed in Figs. (7a) and (7c). It is not considered in the calculation of the mean frequency because of a possible perturbation occurred.

6. CONCLUSION

Increasing the groove width, the vaporized fuel mass flux augments, consequently the flame height increases, imposing a larger region under the influence of the buoyant force. The vortices, generated at the base of the flame, are detached and meanwhile displaced along the flame they are grown. When they reach the center of the flame, it is squeezed and stretched, which produce a local flame extinction, generating the puffing phenomenon. The results confirm that as wider the flame is, as longer is the extinction and as lower puffing frequency.

Decreasing the groove width, the flame flickering takes place of the the puffing phenomenon. The flame height decreases and the vortices displacement time decreases, consequently the vortices growth is not enough to cause the flame stretched up to its extinction. The passage of the vortices by the flame tip causes only its oscillation, because of that the flickering frequency is higher than that of puffing.

Due to hydrodynamic instability, the flame surface is disturbed with a spatial average flame height of 67 mm. A simplified model (infinitely fast chemical kinetics, constant transport and thermodynamic coefficients, and unitary Lewis number) is developed which is able to represent qualitatively the flame height with 91mm. Since the simplified model is able to describe qualitatively the experimental results, it will be improved to capture the transient hydrodynamic effects in future works.

7. ACKNOWLEDGEMENTS

The authors would like to acknowledge the academic support from Instituto Federal do Espírito Santo - IFES and Instituto Nacional de Pesquisas Espaciais - INPE.

8. REFERENCES

Buckmaster, J. and Peters, N., 1986. "The infinite candle and its stability - a paradigm for flickering diffusion flames". *Proceedings of the Combustion Institute*, Vol. 21, pp. 1829–1836.

Burke, S.P. and Schumann, T.E.W., 1928. "Diffusion flames". *Ind. Eng. Chem.*, Vol. 20, pp. 998–1009.

Cetegen, B.M. and Kasper, K.D., 1996. "Experiments on the oscillatory behavior of buoyant plumes of helium and helium-air mixtures". *Phys. Fluids*, Vol. 8, pp. 2974–2984.

Chamberlin, D.S. and Rose, A., 1948. "The flicker of luminous flames". *Proceedings of the Combustion Institute*, Vol. 1-2, pp. 27–32.

Chen, L.D., Seaba, J.P., Roquemore, W.M. and Goss, L.P., 1988. "Buoyant diffusion flames". *Proceedings of the Combustion Institute*, Vol. 22, pp. 677–684.

Fachini, F.F., 1999. "An analytical solution for the quasi-steady droplet combustion". *Combust. Flame*, Vol. 116, pp. 302–306.

Fachini, F.F., Liñán, A. and Williams, F.A., 1999. "Theory of flame histories in droplet combustion at small stoichiometric fuel-air ratios". *AIAA J.*, Vol. 37, pp. 1426–1435.

Fachini, F.F., 2007. "Extended Shvab-Zel'dovich formulation for multicomponent-fuel diffusion flames". *Int. J. Heat Mass Transf.*, Vol. 50, pp. 1035–1048.

Jiang, X. and Luo, K.H., 2000. "Combustion-induced buoyancy effects of an axisymmetric reactive plume". *Proceedings of the Combustion Institute*, Vol. 28, pp. 1989–1995.

Liegens, A., Neemann, K., Meyer, J. and Schreiber, M., 1996. "Instability of diffusion flames". *Proceedings of the Combustion Institute*, Vol. 26, pp. 1053–1061.

Lin, C., Wiesenhahn, D. and Penner, S., 1986. "Multiple diffusion flame with rectangular symmetry". *Combust. Flame*, Vol. 65, pp. 215–225.

Liñán, A., 2001. "Diffusion-controlled combustion". In *Mechanics for a New Millenium*, Eds. Aref H. and Philips J.W., Kluver Academic Publishers, Netherlands, pp. 487–502.

Liñán, A. and Williams, F.A., 1993. *Fundamental Aspects of Combustion*. Oxford University Press, Oxford.

Liu, C., Ding, L., Jangi, M., Ji, J., Yu, L. and Wan, H., 2020. "Experimental study of the effect of ullage height on flame characteristics of pool fires". *Combustion and Flame*, Vol. 216, pp. 245–255.

Liñan, A., Vera, M. and Sánchez, A.L., 2015. "Ignition, liftoff, and extinction of gaseous diffusion flames". *Annu. Rev. Fluid Mech.*, Vol. 47, pp. 293–314.

Maxworthy, T., 1999. "The flickering candle: transition to a global oscillation in a thermal plume". *J. Fluid Mech*, Vol. 390, pp. 297–323.

Moreno-Boza, D., Coenen, W., Sevilla, A., Carpio, J., Sánchez, A.L. and Liñán, A., 2016. "Diffusion-flame flickering as a hydrodynamic global mode". *Journal of Fluid Mechanics*, Vol. 798, p. 997–1014.

Moreno-Boza, D., Coenen, W., Carpio, J., Sánchez, A.L. and Williams, F.A., 2018. "On the critical conditions for pool-fire puffing". *Combustion and Flame*, Vol. 192, pp. 426–438.

Shvab, V.A., 1948. "The relationship between the temperature and velocity fields in a gaseous flame". *In Research on Combustion Processes in Natural Fuel (ed. G. F. Knorre)*, p. pp. 231–248.

Zeldovich, Y.B., 1951. "On the theory of combustion of initially unmixed gases".